ORIGINAL PAPER

Simulation of a cellulose fiber in ionic liquid suggests a synergistic approach to dissolution

Barmak Mostofian · Jeremy C. Smith · Xiaolin Cheng

Abstract Ionic liquids dissolve cellulose in a more efficient and environmentally acceptable way than conventional methods in aqueous solution. An understanding of how ionic liquids act on cellulose is essential for improving pretreatment conditions and thus detailed knowledge of the interactions between the cations, anions and cellulose is necessary. Here, to explore ionic liquid effects, we perform all-atom molecular dynamics simulations of a cellulose microfibril in 1-butyl-3-methylimidazolium chloride and analyze site–site interactions and cation orientations at the solute–solvent interface. The results indicate that Cl^- anions predominantly interact with cellulose surface hydroxyl groups but with differences between chains of neighboring cellulose layers, referred to as center and origin chains;

Cl^- binds to C3-hydroxyls on the origin chains but to C2- and C6-hydroxyls on the center chains, thus resulting in a distinct pattern along glucan chains of the hydrophilic fiber surfaces. In particular, Cl^- binding disrupts intrachain O3H–O5 hydrogen bonds on the origin chains but not those on the center chains. In contrast, $Bmim^+$ cations stack preferentially on the hydrophobic cellulose surface, governed by non-polar interactions with cellulose. Complementary to the polar interactions between Cl^- and cellulose, the stacking interaction between solvent cation rings and cellulose pyranose rings can compensate the interaction between stacked cellulose layers, thus stabilizing detached cellulose chains. Moreover, a frequently occurring intercalation of $Bmim^+$ on the hydrophilic surface is observed, which by separating cellulose layers can also potentially facilitate the initiation of fiber disintegration. The results provide a molecular description why ionic liquids are ideal cellulose solvents, the concerted action of anions and cations on the hydrophobic and hydrophilic surfaces being key to the efficient dissolution of the amphiphilic carbohydrate.

B. Mostofian · J. C. Smith · X. Cheng (✉)
Oak Ridge National Laboratory, UT/ORNL Center for Molecular Biophysics, Oak Ridge, TN 37830, USA
e-mail: chengx@ornl.gov

B. Mostofian
Graduate School of Genome Science and Technology, The University of Tennessee, Knoxville, TN 37996, USA

J. C. Smith · X. Cheng
Department of Biochemistry, Cellular and Molecular Biology, The University of Tennessee, Knoxville, TN 37996, USA

Introduction

The use of ionic liquid (IL) mixtures for the non-derivatized modification of cellulosic material and for

the dissolution of lignocellulosic biomass shows promise as a component of the development of a sustainable and economic biofuel industry (Gericke et al. 2012; Langan et al. 2011; Sun et al. 2011). Due in part to their thermal stability and reusability, ILs have become attractive alternatives to traditional cellulose solvents such as nitrate or aqueous alkali containing solvents (Swatloski et al. 2002; Zavrel et al. 2009; Zhu et al. 2006). Moreover, the application of ILs outperforms common methods of pretreatment, making cellulose more prone to deconstruction during the subsequent process of saccharification (Alvira et al. 2010; Liu and Chen 2006). Enhanced turnover rates of enzymatic hydrolysis arise probably from better accessibility of the polymer to enzymes after treatment with ILs (Dadi et al. 2006; Kim et al. 2010). Characterization of the pretreated and reprecipitated cellulose, via scanning electron microscopy and X-ray diffraction among other techniques, has indicated structural transformation (Dadi et al. 2007; Li et al. 2010), which manifests itself as greater delignification and reduced crystallinity of cellulose. Depending on the source of biomass, and thus on its lignin content, as well as on the pretreatment temperature, conversion of cellulose I (Nishiyama et al. 2002, 2003) to cellulose II (Langan et al. 1999, 2001) upon IL treatment and recrystallization has been observed (Cheng et al. 2011; Samayam et al. 2011). The latter cellulose allomorph is known to be more readily digestible by hydrolyzing enzymes (Chen et al. 2007; Chundawat et al. 2011).

Within the large group of ILs, those with a cation containing an imidazole group and a short alkyl-chain are most effective in interacting with carbohydrate substrates in general and in dissolving cellulose in particular (El Seoud et al. 2007; Heinze et al. 2008; Zhang and Chan 2010). A prominent example of these is 1-butyl-3-methylimidazolium chloride (BmimCl), an IL often used for the non-derivatized dissolution of cellulose (Moulthrop et al. 2005; Rinaldi et al. 2008). However, in order to better exploit ILs as an efficient and more economic solvent system for biomass pretreatment, the mechanism by which they act on the solute needs to be better understood. To this end, there has been some effort in designing new ILs and effects of their application to cellulose have been discussed (Fukaya et al. 2010; Liu et al. 2010a; Ohira et al. 2012; Sellin et al. 2010). It has been widely accepted that, in order to disintegrate the cellulose fibril structure, a good cellulose solvent must break the inter- and intramolecular hydrogen bonds between and within glucan chains (BeMiller and Whistler 1996; Zhang et al. 2002). This general viewpoint, however, has recently been challenged in several reports claiming that the role of hydrophobic interactions in the solubility of cellulose had been underestimated (Lindman et al. 2010; Medronho et al. 2012). Indeed, potential of mean force calculations for the separation of cellooligomers using molecular dynamics (MD) simulation have suggested that hydrophobic interactions contribute favorably to stabilizing a crystal-like stacked structure (Bergenstrahle et al. 2010). Moreover, when considering the intricate cellulose solubility problem, the amphiphilic character of cellulose polymers should not be overlooked. There is some agreement that the amphiphilic nature of cellulose affects its structural properties—a concept referred to as the "Lindman Hypothesis" (Glasser et al. 2012). Therefore, in order to simultaneously weaken the solute's hydrophobic and hydrogen bond interactions and facilitate dissolution in a more effective way, a good cellulose solvent should have both polar and non-polar groups.

Atomic-detail MD simulations have proven to be a powerful tool for the analysis of the structure and dynamics of cellulose in aqueous and IL solutions (Kowsari et al. 2008; Margulis et al. 2002; Raju and Balasubramanian 2010; Ramadugu et al. 2009; Youngs et al. 2007). Studies of cellulose oligomers have revealed more favorable solute–solvent interaction energies and increased conformational flexibility of glucan chains in IL solutions than in aqueous solutions (Liu et al. 2010b). Similarly, MD simulations of a cellulose oligomer in binary solvent systems with varying IL/water ratios characterized molecular interactions between cations, anions, water and cellulose during precipitation after IL pretreatment (Liu et al. 2011). Recently, a computational study has shown more favorable free energies for peeling off one glucan chain from a cellulose crystal in BmimCl than in water (Cho et al. 2011; Gross et al. 2012). Using a two-phase thermodynamic model, the calculation suggested reduced solvent entropy loss upon dissolution in BmimCl. Moreover, by dissecting interaction forces based on a coarse-grained scheme, this work demonstrated stronger interaction of the cellulose hydroxyl and hydroxymethyl groups with the cation or the anion than with water. Such a coarse-grained description focuses on interactions between

different functional groups, but cannot examine favored orientations of the larger cation molecules on the fiber surface and underlying atomistic site–site interactions. In order to understand the initial steps of cellulose dissolution in ILs and to highlight the mechanism or mode of action by which cations and anions may initiate the disintegration of a cellulose fiber, it is essential to simulate and analyze at atomic resolution.

To the above end, we have conducted all-atom MD simulations of a 36-chain cellulose microfibril solvated in BmimCl. Computational limitations on the accessible timescale are such that no complete dissolution of the cellulose fiber or penetration of solvent ions into the fiber interior is expected to occur in the simulations. Rather, the calculations permit observation of early stages of the process at atomic detail. The goal is to gain insight into the interaction patterns of initial solute–solvent contacts, and, in particular, the positioning of the IL cations and anions during the initial steps of dissolution. Previously, we have shown preferential accumulation of solvent ions on the different fiber surfaces and conformational variability of the solvent-exposed hydroxymethyl groups (Mosto-fian et al. 2011). Here, we present longer simulations and a detailed analysis of site–site contacts and favored orientations of solvent molecules around cellulose surfaces. The results indicate that both cations and anions indeed play active roles in the onset of cellulose dissolution. While Cl^- disrupts accessible intramolecular cellulose hydrogen bonds, $Bmim^+$ positions itself on top of hydrophobic surfaces in a stacking fashion and also intercalates in between cellulose strands on hydrophilic surfaces in a process likely to facilitate the initiation of cellulose deconstruction.

Methods

MD simulation

A 36-chain Iβ-cellulose crystal fiber (Fig. 1) with 20 glucose units per chain was solvated in an equilibrated cubic box of BmimCl ion pairs. After deleting overlapping molecules and energy minimization, the fiber was surrounded by ∼25 Å of solvent on both sides along the direction of its polymerization axis and by 40–60 Å of clearance around the other surfaces.

These large values correspond to a few head-to-tail distances of BmimCl, thus allowing for a reliable analysis of solvent structures close to the fiber surfaces. The total number of atoms is 182,070. GLYCAM06 (Kirschner et al. 2008) molecular mechanics force field parameters were used for the cellulose. BmimCl parameters had been developed previously (Liu et al. 2004) and partial charges were assigned through fitting to electrostatic potentials computed at the Hartree–Fock level with 6–31G* basis set using GAUSSIAN (2009). Simulations were performed and analyzed with GROMACS (Hess et al. 2008). Long-range electrostatic interactions were calculated using the particle-mesh Ewald summation (Darden et al. 1993; Essmann et al. 1995) with a real-space cut-off at 12 Å. Van der Waals interactions were cut off at 10 Å.

The system was equilibrated to the target temperature of 450 K which corresponds to the biomass pretreatment conditions with an IL. The temperature was maintained by velocity rescaling with a stochastic term to ensure proper sampling (Bussi et al. 2007). After equilibrating the density with a short NPT simulation applying the Berendsen barostat (Berend-sen et al. 1984), the system was subjected to 5 ns of NVT equilibration. The production run was performed for over 100 ns with a time step of 2 fs in the NVT ensemble. Bonds to hydrogen atoms were constrained using the LINCS algorithm (Hess et al. 1997).
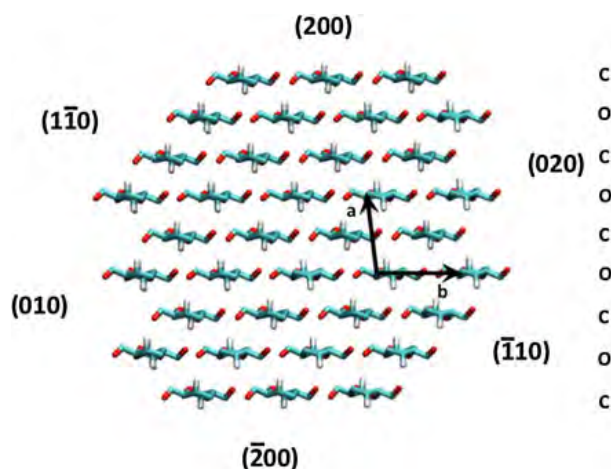
Fig. 1 A cross-section view of a 36-chain microfibril model of the cellulose Iβ allomorph. Axes **a** and **b** define the monoclinic unit cell. The six faces are assigned Miller Indices. Layers consisting of center (C) or origin (O) chains are labeled on the right

Cation orientations

To identify the arrangement of Bmim$^+$ cations around surface glucose monomers, a set of three-dimensional Euler angles (θ_x, θ_y, θ_z) was derived for every cation with a maximum imidazole ring-center to pyranose ring-center distance of 7 Å. Euler angles were computed from rotational matrices and correspond to successive rotations of the cations around the z-, y-, and x-axis of their laboratory coordinate system (Fig. 2a) in order to transform them to the reference coordinate system of the adjacent glucose unit (Fig. 2b). Three-dimensional histograms were derived with a bin size of 7.2° (50 bins) in each direction of the orientation space. These orientation histograms were normalized and smoothed with a three-dimensional Gaussian function in order to remove statistical noise. Histograms were created with MATLAB (2011) and orientations illustrated with VMD (Humphrey et al. 1996). Cation orientations were evaluated with respect to the 16 central glucose units of any surface glucan chain. Terminal cellobiose units were neglected in this analysis and in the computation of all
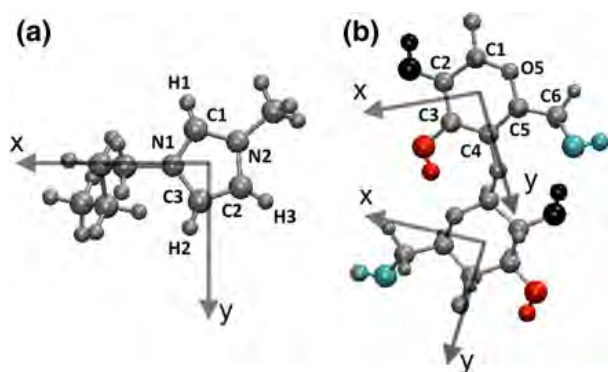
Fig. 2 Definition of coordinate systems for solvent cations and solute monomers. **a** The laboratory coordinate system is defined for Bmim$^+$ cations with the x–y-plane as the plane of the imidazole ring (that is the plane defined by N1, N2, and C2). This view is along the negative z-axis. The x-axis is defined along the connection of the ring-center to the butyl group. The y-axis is defined to be perpendicular to the x- and z-axes as shown here. **b** The reference coordinate system is defined for glucose monomers with the x–y-plane as the plane of the pyranose ring (that is the plane defined by C2, C4, and O5). This view is along the negative z-axis. The y-axis is defined along the connection of the ring-center and the glycosidic bond. The x-axis is defined to be perpendicular to the y- and z-axes as shown here. For any monomer of a cellobiose unit, functional groups appear on different sides around the defined axes and thus both types are displayed here. The cellobiose hydroxyl groups of C2 (*black*), C3 (*red*), and C6 (*cyan*) are colored. (Color figure online)

radial distribution functions in order to eliminate potential artefactual effects due to their greater flexibility.

Results and discussion

The starting cellulose crystal consists of 36 chains arranged in nine layers. Based on their placement in the monoclinic unit cell of the Iβ allomorph, cellulose strands from neighboring layers are referred to as center and origin chains, as illustrated in Fig. 1, which are non-equivalent in terms of their environment (Nishiyama et al. 2002). The fiber has six faces which can be annotated by Miller Indices as they correspond to lattice planes of the underlying crystal. Two of these, the (200) and ($\bar{2}$00) surfaces, are generally referred to as hydrophobic, while the remaining four surfaces, (1$\bar{1}$0), ($\bar{1}$10), (010), and (020), all expose the equatorial hydroxyl groups to the surroundings and are thus referred to as hydrophilic. We also denote parallel surfaces from opposite sides of the fiber as "corresponding surfaces" as their shape is identical to each other and different from the other surfaces. There are three pairs of corresponding surfaces in the given fiber structure. Any two corresponding surfaces expose hydroxyl groups or ring hydrogens to the solvent in the same way. To explore the behavior of solvent and its possible effect on a cellulose fiber, we characterize contacts between BmimCl and the cellulose surfaces. In the following, we discuss the structure of Bmim$^+$ and Cl$^-$ in proximity to three of the six fiber surfaces. Only one surface from any pair of corresponding surfaces is considered, namely the hydrophobic (200) and the hydrophilic (1$\bar{1}$0) and (010) faces. As the analysis of spatial density distributions in earlier studies has revealed, the solvent arranges itself in a symmetric fashion around cellulose fibers during the initiation phase of dissolution (Gross and Chu 2010; Matthews et al. 2006; Mostofian et al. 2011). It has been shown that solvent components such as Bmim$^+$ and Cl$^-$ occupy distinct sites on cellulose surfaces, for example the space between two cellulose chains, with the same density on any two corresponding surfaces. Therefore, it can be presumed that similar interaction between cellulose and BmimCl is taking place at the analogous positions on corresponding surfaces, and considering only one surface from any corresponding surface pair in our analyses thus suffices to provide

information on all crucial solute–solvent interactions. It should also be noted that the symmetrical distribution of solvent around the cellulose fiber indicates convergence of the MD simulation for the analysis of solute–solvent interactions.

Radial distribution functions (RDFs) are instrumental for identifying dominant short-range contacts or mid-range structural order in liquids. We calculated RDFs for Cl^- with respect to solvent-exposed hydrogen atoms from the C2-, C3-, and C6-hydroxyl groups (see Fig. 2b), which are the sites of greatest Cl^- accumulation. Fig. S1a (Supplementary Information) reveals that highest peaks, and thus the strongest interactions, are between the anions and the hydrophilic $(1\bar{1}0)$ surface, with a site–site separation of 2–3 Å. In contrast, the RDFs of the ring and methyl hydrogens of the cation with respect to the solvent-exposed oxygen atoms of the cellulose hydroxyl groups show broad profiles of low intensity (Fig. S1b), suggesting that $Bmim^+$ does not accumulate around hydroxyl groups of the cellulose surfaces. However, this analysis of site–site RDFs does not exclude the possibility that the rather bulky cation may

have a preferred way of approaching and aligning itself at cellulose surfaces. Indeed, g(r) profiles for the center of mass of the imidazole ring atoms with respect to the pyranose rings of the central glucan chains on different cellulose surfaces, reveal a slight minimum at around 7 Å, particularly for the $(1\bar{1}0)$ and the (010) surfaces (Fig. S2). Hence, we performed an orientational analysis of those $Bmim^+$ cations located within 7 Å of surface pyranose ring centers. In the remainder of this section, we present the orientations of $Bmim^+$ relative to the glucose units on the three different surfaces of the cellulose fiber, together with RDFs for Cl^- in greater detail.

Solvent structure around the hydrophobic (200) surface

To assess the extent to which Cl^- anions interact with the hydrophobic (200) surface, we computed RDFs with respect to the hydrogens of the hydroxyl groups in the three surface chains (Fig. 3a, b). In order to focus on interactions specific to this surface, not all hydroxyls from the two border chains were considered
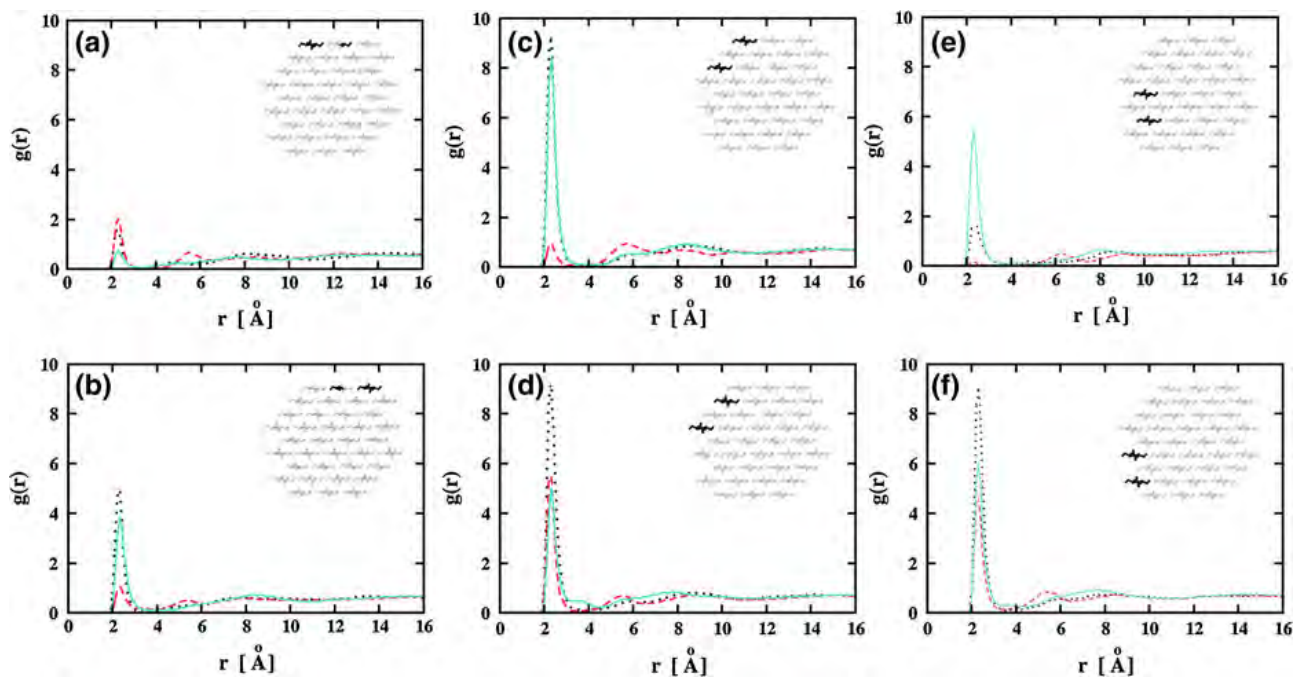
Fig. 3 Radial distribution functions (RDFs) of Cl^- anions around cellulose surface hydroxyl groups. Each profile describes a site–site RDF between Cl^- and hydrogen atoms of the C2- (*dotted black*), C3- (*dashed red*), or C6-hydroxyl (*solid cyan*) on the highlighted glucan chains (*inset*). RDFs are shown with respect to **a** hydroxyl groups on the (200) surface showing toward the (020) surface, **b** hydroxyl groups on the (200) surface showing toward the $(1\bar{1}0)$ surface, **c** center chain hydroxyl groups on the $(1\bar{1}0)$ surface, **d** origin chain hydroxyl groups on the $(1\bar{1}0)$ surface, **e** center chain hydroxyl groups on the (010) surface, and **f** origin chain hydroxyl groups on the (010) surface. (Color figure online)

as reference sites, as these may also be assigned to a neighboring surface. Hence, only those hydroxyls on the two border chains that point toward the middle chain on (200) were included, while on the middle chain all hydroxyls were considered. Moreover, RDFs with respect to hydroxyl groups pointing toward the neighboring (020) surface are combined in Fig. 3a while those toward ($1\bar{1}0$) are combined in Fig. 3b. The reason for averaging these RDFs is that the individual profiles were found to be of comparable shape. As shown in these two plots, Cl^- preferentially appears around the C2- and C6-hydroxyls pointing toward the (020) surface (dotted black and solid cyan profiles in Fig. 3b). The g(r) profiles for the corresponding C3-hydroxyl (dashed red in Fig. 3b) as well as for all hydroxyls extending toward the ($1\bar{1}0$) surface (Fig. 3a) show a much smaller peak.

The reason for this differential interaction pattern within one layer of cellulose chains lies in the fact that, during the course of the simulation, the center and origin chains tilt clockwise or counter-clockwise, respectively, with respect to the polymerization axis, as observed in previous fiber simulations (Matthews et al. 2011). Analysis of the tilt angle for any cellulose chain reveals an average value of approximately $+10°$ for center chains and $-10°$ for origin chains, respectively (Fig. S3). As a result, the (200) surface chains tend to expose hydroxyl groups on one side to the solvent while hiding the other side from the solvent. Nevertheless, even among the solvent-exposed C3-hydroxyls, the RDF shows a relatively lower peak (dashed red profile in Fig. 3b) suggesting that the intrachain O3H–O5 hydrogen bonds remain largely intact. Indeed, the occupancy of these hydrogen bonds over the course of the entire simulation is only slightly lower than that in the fiber core (Fig. S4).

The differential interaction of Cl^- with C2- and C6-hydroxyls on the hydrophobic surface is also
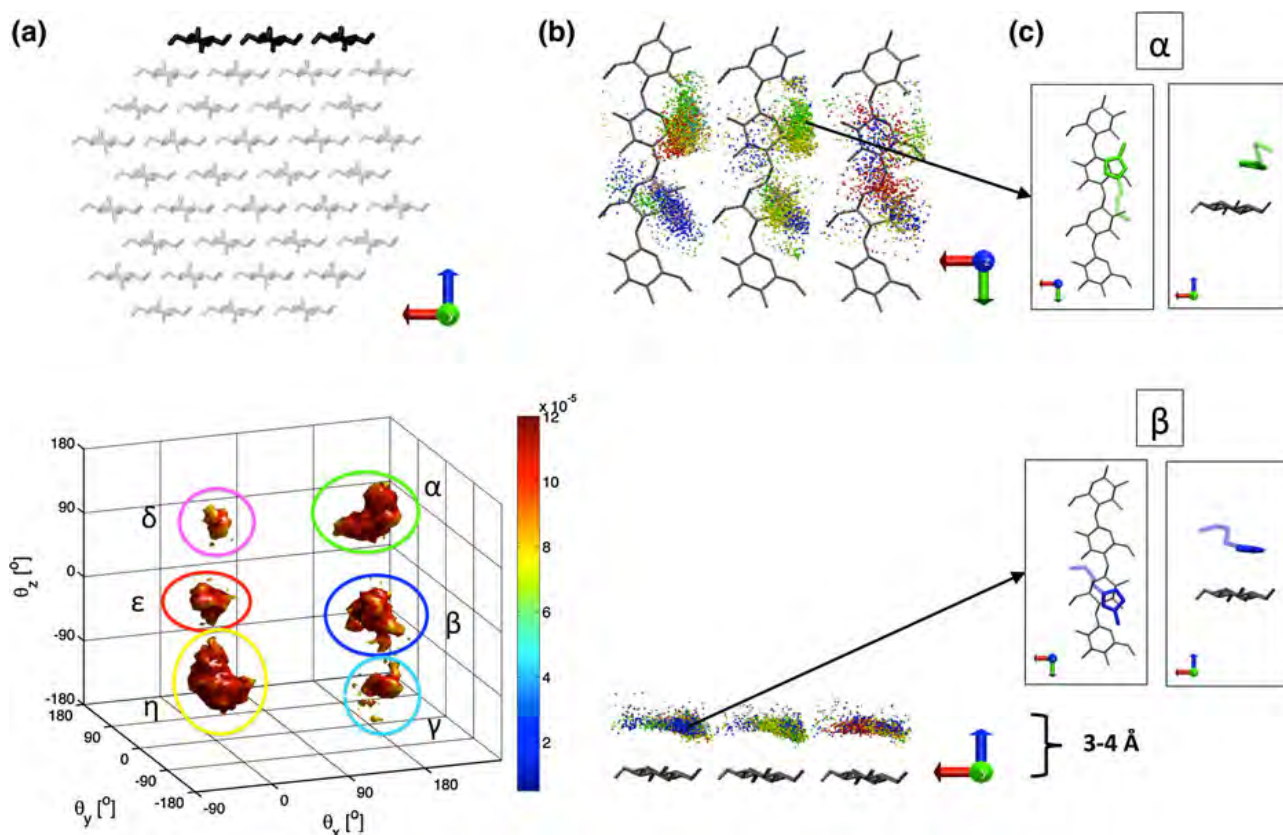
Fig. 4 Analysis of solvent cation orientations with respect to solute monomers on the (200) surface. **a** Orientations are presented for cations around the cellulose (200) surface (*top*). Six peaks in the histogram are identified and shown as distinct regions in orientation space (α, β, γ, δ, ε, η) (*bottom*). **b** The positions of all cation ring-centers with respect to closest glucose monomers are visualized in a top view and a side view of the surface. *Colors* correspond to histogram peaks in (**a**). The average orientation and separation for the two most populated histogram peaks (α and β) is shown explicitly. (Color figure online)

illustrated by computing three-dimensional spatial densities (Fig. S5a–c). Chains bordering on neighboring surfaces show solvent density not only on top but also on the respective sides of the glucan chains in these averaged distribution images.

The spatial distributions in Fig. S5a–c also reveal that Bmim$^+$ cations do not have a specific interaction site on the (200) surface, as no ring hydrogen density peaks (meshed contours) are visible around any surface sites. On the other hand, an orientational analysis for Bmim$^+$ indicates that the cations do have a preferred alignment at this cellulose surface. The corresponding histogram (Fig. 4a) shows several prevailing regions in orientation space which are clustered into six groups (α, β, γ, δ, ε, η). Figure 4b visualizes the positions of all cation ring-centers from these preferred orientations with respect to the nearest pyranose ring center in a top and a side view of the (200) surface. The bulk of these most prevalent orientations is found on top of the glucose rings, indicating that Bmim$^+$ avoids positioning in between neighboring strands or over the glycosidic bonds. Instead, the cation is mainly positioned over the pyranose rings in the favored orientations determined with respect to the glucose monomer.

In Fig. 4c, the average arrangement and separation with reference to the closest glucose ring is visualized for structures from the two most populated groups of preferred orientations in Fig. 4a. Averages of all six high-occupancy orientation clusters are given in Fig. S6a. Bmim$^+$ cations are found to align themselves by stacking with the imidazole rings parallel to the closest glucose rings. The Bmim$^+$ tail and head groups do not have preferred directions, and this is also indicated by the observation that $θ_z$ adopts several values for the highlighted groups while $θ_x$ is either ~0° or ~180° and $θ_y$ is ~0°, signifying parallel arrangement of the imidazole and glucose ring planes. For all high-occurrence orientations, the separation of the imidazole ring center from the closest pyranose ring center is strictly between 3 and 4 Å.

The above results indicate that cation rings stack against the hydrophobic (200) surface. To gain a quantitative understanding of this stacking interaction, we decomposed the interaction potential energy between any Bmim$^+$ cations and the cellulose fiber into electrostatic (E_{coul}) and van der Waals (E_{vdW}) contributions for each of the preferred orientations which are shown in Fig. 5a. On average, the computed E_{vdW} of below -10 kcal/mol is clearly lower than E_{coul}. This indicates that the stacking of cation rings at this

Fig. 5 Decomposition of the interaction potential energy between solvent cations and cellulose into Coulombic (*top bar*) and van der Waals (*bottom bar*) energy; cations assigned to the histogram peaks in Figs. 4, 6, or 7 are taken into consideration for **a** the (200), **b** the (1$\bar{1}$0), and **c** the (010) surface, respectively
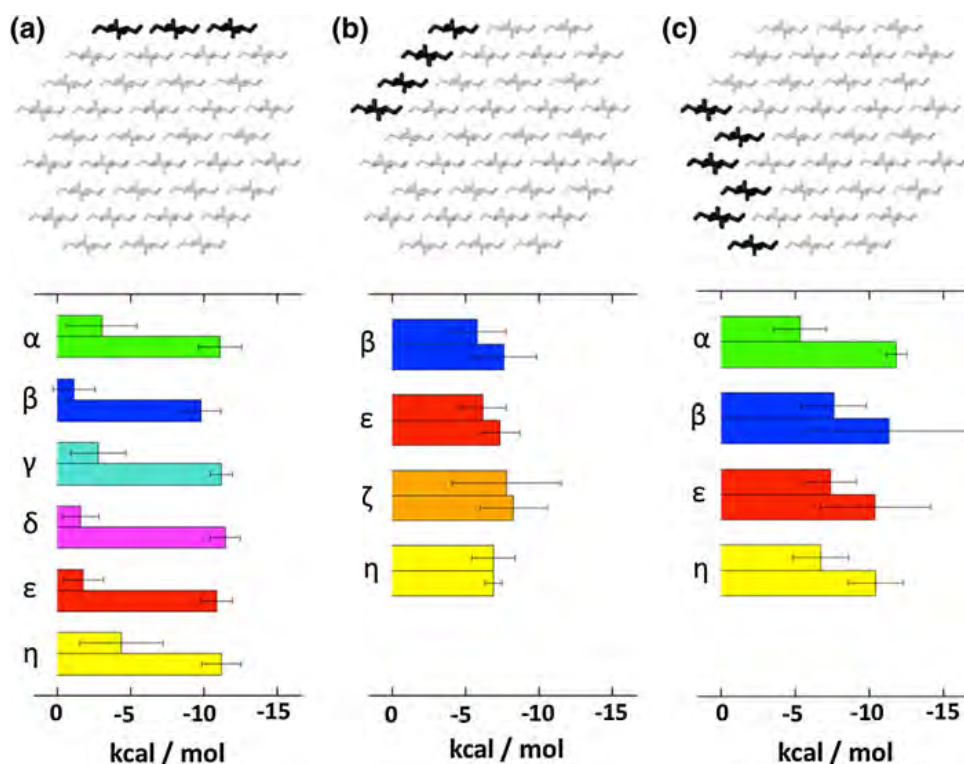
interface involves mainly non-polar interaction between the cellulose and the Bmim$^+$ cations. This may compensate stacking interactions between cellulose layers, facilitating the transition from a compact crystal structure to detached cellulose chains. Indeed, X-ray diffraction studies on fibers from ramie cell walls treated with EmimAc, an IL with a cation similar to BmimCl, have shown a reduced and broadened (200) reflection peak compared to untreated cellulose (Lucas et al. 2011), interpreted as a reduction of cellulose stacking interactions due to IL treatment. In our simulations, it is noticeable that both the Cl$^-$ anions and Bmim$^+$ cations are engaged in attacking the hydrophobic (200) surface in distinct, and yet complementary, ways.

Solvent structure around the hydrophilic $(1\bar{1}0)$ surface

The fiber $(1\bar{1}0)$ face is referred to as hydrophilic because hydroxyl and hydroxymethyl groups on this surface are exposed to the solvent. Since individual RDF profiles of Cl$^-$ with respect to hydroxyl hydrogens on center or origin chains are of comparable shape, they are combined into one plot for the center chains (Fig. 3c) and one for the origin chains (Fig. 3d). These profiles show that Cl$^-$ avoids the C3-hydroxyl while accumulating around the C2- and C6-hydroxyl groups on center chains. For the origin chains, g(r) also peaks at ~ 3 Å for Cl$^-$ around hydrogens on C3, indicating direct interaction. This is further confirmed by the much lower intrachain O3H–O5 hydrogen bond occupancy for solvent-exposed origin chains on this surface (Fig. S4), the mean percentage values being 25.2 and 39.4 %, respectively, for the two origin chains while for the center chains the corresponding occupancy values reach ~ 80 %, comparable to those for the fiber core. Calculating the average solvent-accessible surface area (SASA) per monomer for surface hydroxyl groups leads to the same conclusion, i.e. that C3-hydroxyl groups on center chains are not available for direct interaction with the solvent. As shown in Fig. S3, hydrogen atoms from the C3-hydroxyl group contribute to the SASA of the center chains five times less than to the origin chains while the corresponding SASA values for the C2- or C6-hydroxyls remain fairly constant between the different chains. This

analysis shows how accessible these surface hydroxyls can be to solvent molecules if not hydrogen bonded to the solute as in the case of the C3 group on center chains.

While in the initial crystal structure the two types of glucan chains differ only with respect to their chemical environment, the clockwise and counter-clockwise tilting in the simulation (Fig. S3) as well as the differential hydrogen bonding (Fig. S4) result in characteristic hydrophilic surfaces with alternating center and origin chains exposing distinct sites for interaction with solute molecules. As a result, Cl$^-$ anions and Bmim$^+$ cations surrounding the solvent-exposed hydroxyl groups arrange differently on different chains of the $(1\bar{1}0)$ surface.

Spatial distributions give an averaged three-dimensional illustration of the interaction between anions and C3-hydroxyls on origin chains and the absence of Cl$^-$ density contours at corresponding positions of center chains (Fig. S5c–f). Interestingly, these images of average density also reveal that Bmim$^+$ cations concentrate along the cellulose strands of the $(1\bar{1}0)$ surface, albeit at lower probabilities than Cl$^-$. Bmim$^+$ tends to occupy the space on the cellulose surface in which Cl$^-$ is less accumulated, that is, in particular around the hydrogen-bonded C3-hydroxyl on the center chains (Fig. S5c,e), and to some degree around the C2- and C6-hydroxyl groups on the origin chains (Fig. S5d). Hence, anions and cations appear in an alternating fashion along the chains of the hydrophilic $(1\bar{1}0)$ surface, and in particular its center chains. The bottom origin chain on this surface shows density contours mainly beneath and above the pyranose ring plane (Fig. S5f) due to its intermediate character as a border chain to the neighboring surface.

In Fig. 6a, four relatively concentrated regions imply strong orientational preference for Bmim$^+$ on the $(1\bar{1}0)$ surface. These preferred orientations are mainly found in between neighboring cellulose strands on the $(1\bar{1}0)$ surface (Fig. 6b, c). For the two most prevalent orientations (denoted β and ε), the average arrangement and separation from the nearest pyranose ring center show that the cation indeed intercalates between neighboring chains. Moreover, in both orientations, the imidazole rings are aligned in a similar way with respect to the fiber surface. The head or tail group of Bmim$^+$ points to opposite directions along the main fiber axis and the C1–H1 group of the

imidazole ring points away while the C2–H2 and C3–H3 groups face the interchain space of the hydrophilic surface in both orientations. The two remaining cation orientations (see Fig. S6b) are of much lower probability and may be considered as intermediate structures for a transition between orientations β and ε. Decomposition of the interaction potential energy between Bmim$^+$ and cellulose reveals comparable E_{coul} and E_{vdW} values (Fig. 5b). The average Coulombic contribution is 4.2 kcal/mol lower and the average van der Waals energy is 3.3 kcal/mol higher than the corresponding interaction energies for the hydrophobic (200) surface. This indicates that cations can also interact with the hydrophilic surface of cellulose through favorable electrostatic interaction.

It should be noted that the intercalation of Bmim$^+$ cations is facilitated by the above-mentioned clockwise and counter-clockwise tilt of center and origin chains, respectively, which results in surface residues and functional groups moving against (when the origin layer is on top) or away from each other (when the center layer is on top). As a result, two grooves open on this surface that further help Bmim$^+$ to penetrate. This intercalation of Bmim$^+$ and the selective disruption of O3H–O5 hydrogen bonds on the origin chains by Cl$^-$ both indicate that cations and anions of the IL can interact with the hydrophilic $(1\bar{1}0)$ surface in distinct ways. These interactions may be primary steps in the dissolution of a cellulose fiber.

Solvent structure around the hydrophilic (010) surface

The fiber (010) face contains voids which can be occupied by solvent molecules. The voids are defined by adjoining origin chains above and beneath as well as the side groups from the center chains. Consequently, this fiber surface does expose pyranose ring
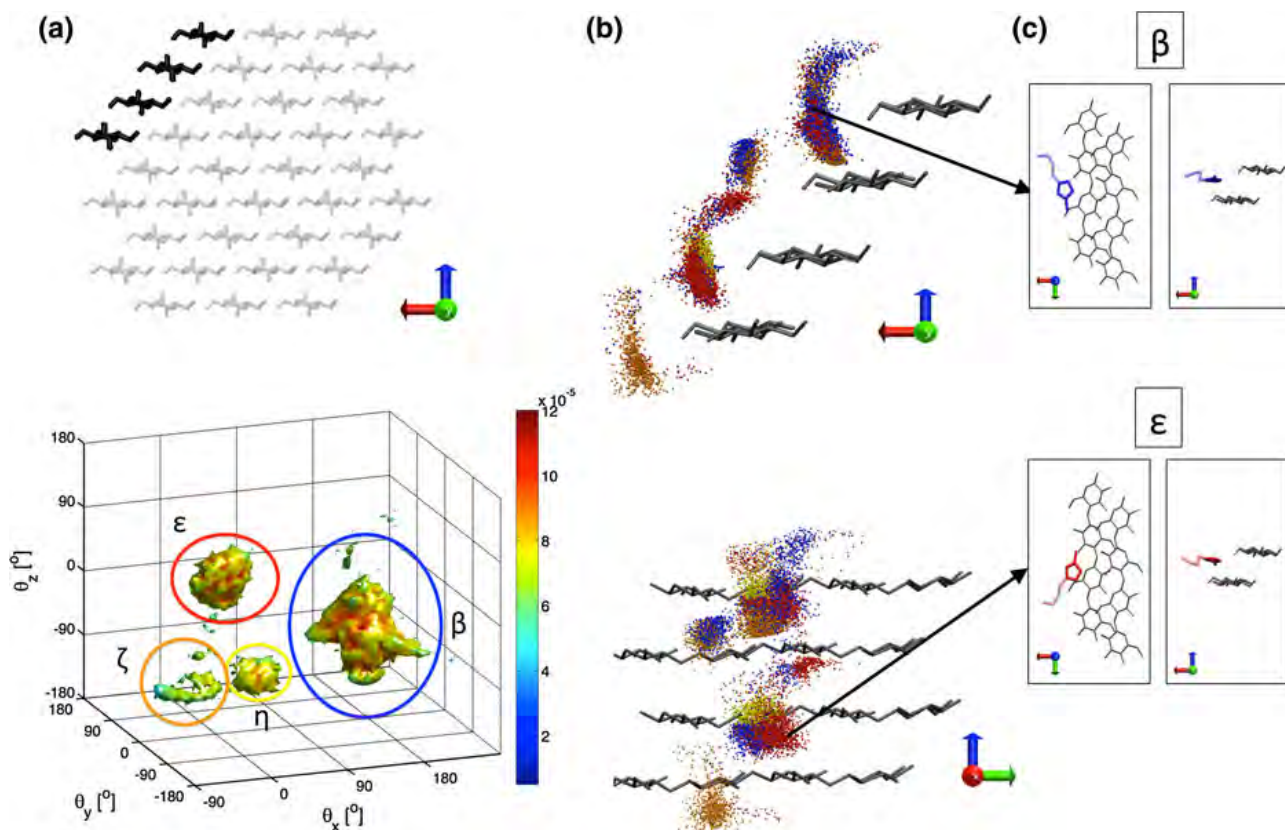
Fig. 6 Analysis of solvent cation orientations with respect to solute monomers on the $(1\bar{1}0)$ surface. **a** Orientations are evaluated for cations around the cellulose $(1\bar{1}0)$ surface (*top*). Four peaks in the histogram are identified and shown as distinct regions in orientation space (β, ε, ζ, η) (*bottom*). **b** The positions of all cation ring-centers with respect to closest glucose monomers are visualized in two different side views of the surface. *Colors* correspond to histogram peaks in (**a**). The average orientation and separation for the two most populated histogram peaks (β and ε) is shown explicitly. (Color figure online)

hydrogens to the solvent, but due to the greater exposure of hydroxyl groups, it is also referred to as hydrophilic. The bottom center chain, which borders on the hydrophobic ($\bar{2}00$) face, is neglected in the following analysis of solvent distributions due to its intermediate character as a border chain between two different surfaces. RDFs for Cl^- are similar to the other hydrophilic surface. On the center chains, the anions avoid the C3-hydroxyl hydrogen and accumulate mainly around the C6-hydroxyl, while on the protruding origin chains the RDFs show strong peaks for Cl^- around all hydroxyl groups (Fig. 3e, f). The hydrogen on the C6-hydroxyl contributes significantly more to the SASAs of the center chains (on average 25.9 %) than the C2- and C3-hydroxyls (15.3 and 0.3 %) (Fig. S3), which may be the reason for the higher peak of C6-hydroxyls in Fig. 3e. Similar to the interactions between BmimCl and cellulose on the hydrophilic (010) surface, occupancies indicate that

the binding of Cl^- to C3-hydroxyl hydrogens disrupts the intrachain hydrogen bonding OH3–O5 to a greater extent on protruding origin chains than on buried center chains (Fig. S4). Here as well, the anions and cations accumulate in an alternating way around side groups of center chains on this surface (Fig. S5g–j), which is further enhanced by the presence of the surface voids.

Finally, analyzing the arrangement of $Bmim^+$ cations around the (010) surface reveals frequently occurring orientations, of which the two most preferred (orientations β and ε in Fig. 7a) are identical to those on the previously discussed hydrophilic ($1\bar{1}0$) surface, which means that the C1–H1 group of the imidazole ring extends into the solvent. On the hydrophilic (010) surface, however, cations adopt their preferred orientations upon intercalating into the available voids (Fig. 7b, c). The average interaction energies between the cellulose and $Bmim^+$ show
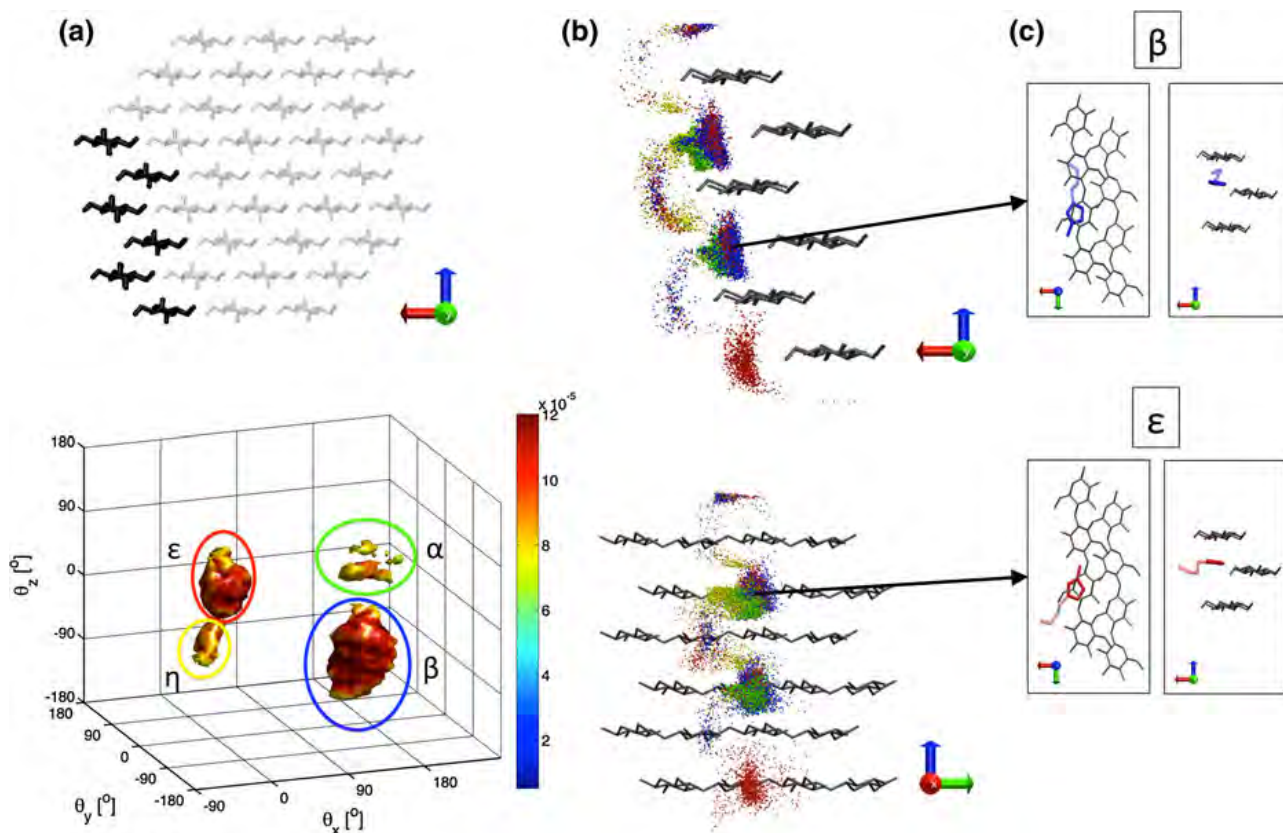
Fig. 7 Analysis of solvent cation orientations with respect to solute monomers on the (010) surface. **a** Orientations are evaluated for cations around the cellulose (010) surface (*top*). Four peaks in the histogram are identified and shown as distinct regions in orientation space (α, β, ε, η) (*bottom*). **b** The positions of all cation ring-centers with respect to closest glucose monomers are visualized in two different side views of the surface. *Colors* correspond to histogram peaks in (**a**). The average orientation and separation for the two most populated histogram peaks (β and ε) is shown explicitly. (Color figure online)

comparable Coulombic interactions as on the other hydrophilic ($1\bar{1}0$) surface and also comparable van der Waals interactions as on the hydrophobic (200) surface (Fig. 5c). The stronger E_{vdw} at this surface compared to the other hydrophilic surface is due to the interaction of cations with the non-polar pyranose rings above and beneath the surface voids.

During the MD simulation we observed several changes in the conformation of the cellulose fiber. The clockwise and counter-clockwise tilt of the center and origin chains gives rise to certain hydroxyl groups being more solvent-exposed than others. In addition, the cellulose fiber twists and swells from the beginning of the simulation. A calculation for the central layer of glucan chains shows that the fiber twists around its polymerization axis by $\sim20°$ on average and the distance between neighboring unit cells in the fiber core increases by approximately 0.3 Å on average along the cell dimension a. All these changes, along with the different orientations of hydroxymethyl groups on center chains compared to origin chains, have been observed before in simulations of Iβ-cellulose fibers (Bergenstrahle et al. 2007; Matthews et al. 2006, 2010, 2011; Mostofian et al. 2011; Yui et al. 2006). Therefore, the solvated fiber behaves as observed before and structural features of the different fiber surfaces allow cellulose to undergo favorable polar and non-polar interactions with the IL.

The significantly higher probability of Bmim$^+$ cations with the C1–H1 group of imidazole rings pointing away from both hydrophilic surfaces examined suggests that these orientations may serve a distinct function. Recent spectroscopic analyses assign a greater acidity to the H1 proton on IL imidazole rings (Muldoon et al. 2001; Reichardt 2005) which means that this site can be considered a better hydrogen bond donor than the other imidazole protons. Therefore, it may seem surprising that the H1 proton points away from the solute in the preferred Bmim$^+$ orientations instead of hydrogen bonding to the hydrophilic cellulose surfaces where exposed hydroxyl oxygens can accept hydrogen bonds. One plausible reason for this may be that all imidazole ring hydrogens are relatively polar due to the delocalized electron system such that the combined interactions of hydrogens H2 and H3 with the hydrophilic fiber surfaces would outweigh the respective interactions of H1 with those surfaces. Alternatively, the observed

orientations could also be stabilized through polar interactions of Bmim$^+$ ring hydrogens with Cl$^-$. As previously reported (Bhargava and Balasubramanian 2007; Gray-Weale 2009; Liu et al. 2004; Urahata and Ribeiro 2005), anions prefer to accumulate around the more polar H1 proton of imidazole. This fact is consistent with the presence of a sharp peak at a smaller distance in the RDF of Cl$^-$ around H1 compared to RDFs of Cl$^-$ around H2 or H3 in simulations of bulk BmimCl (data not shown). Coordination numbers (cn) derived through the integration of the RDF profiles from zero up to the first minimum indicate the slightly preferred interaction of Cl$^-$ with H1 (cn = 1.4) rather than with H2 (cn = 1.2) or with H3 (cn = 1.1). Thus, the intercalation of cations observed in the fiber simulation, in which H1 preferentially faces the solvent while H2 and H3 are oriented toward cellulose, may arise from an interplay of the polar ring hydrogens interacting with anions on one side and surface hydroxyls on the other side.

In order to examine whether the affinity of polar imidazole ring hydrogens to Cl$^-$ or to cellulose surface hydroxyls is the reason for the preferred Bmim$^+$ orientations on the hydrophilic surfaces, we computed the average electrostatic contribution to the interaction potential between these hydrogens and the hydrophilic fiber surfaces or the solvent Cl$^-$ in the respective intercalating orientations (β and ε) and compared these values to those in the structures in which H1 faces the hydrophilic surfaces and H2 and H3 extend toward solvent (Fig. S7). These opposite orientations are not visible as peaks in the orientation histograms of Figs. 6 and 7 because they are sparsely populated (a few hundred structures were evaluated for each of the two surfaces) compared to the preferred orientations. Our calculations reveal, for both of the preferred structures on hydrophilic ($1\bar{1}0$) and (010) surfaces, the average Coulombic interactions between Cl$^-$ and H1 are greater than the sum of such interaction energies for H2 and H3 with the fiber surface. Also, for opposite intercalating orientations, the average interaction energies of H2 and H3 with Cl$^-$ are clearly higher than those between H1 and the respective fiber surface. However, the average sum of the Coulombic interaction energies for polar imidazole hydrogens and fiber surfaces or Cl$^-$ anions is comparable between structures taken from the preferred orientations and those taken from the opposite

orientations (on average, between -16.2 and -19.2 kcal/mol for all six analyzed orientations from the two hydrophilic surfaces). Hence, we can exclude that the preferred orientations observed on the hydrophilic surfaces arise from a higher affinity of the acidic imidazole H1 site for Cl^- or the combination of H2 and H3 interactions with surface hydroxyl groups.

The dominant $Bmim^+$ orientation found on the hydrophilic surfaces can possibly also explain why the alkyl chain length has to be limited to 4–6 carbons for imidazolium-based ILs to be effective in cellulose dissolution (Wang et al. 2012; Zhao et al. 2012). The length of the alkyl chain determines the amphiphilic character of the solvent. The cation studied here contains a butyl tail and the present results suggest that the alkyl chain is restricted to roughly this number, due to structural reasons based on the observed preferred orientations at the fiber $(1\bar{1}0)$ and (010) faces in which the cation tail is positioned parallel to the glucan chain. Cations occurring in proximity to any cellulose surface have an average head to tail distance of ~7.5 Å, which is comparable to the value for cations in bulk BmimCl. This value is smaller than the length of a cellobiose unit (~10.5 Å between linker oxygens) and just smaller than the separation of neighboring C2- and C6-hydroxyls on a glucan chain (~8 Å), which is the preferred site of $Bmim^+$ on center chains of hydrophilic surfaces as discussed above (see Fig. S5). As a consequence, a longer alkyl tail would prevent cations from appearing next to neighboring cellobioses at the same time and would also interfere with Cl^- anions at their cellulose interaction sites, hindering them from penetrating the fiber. The solvent structure around the fiber captured in this study, an alternating occurrence of cations and anions along the glucan chains on the hydrophilic surfaces (in particular the center chains) could not be realized with a longer cation alkyl group.

Inter- and intrachain hydrogen bonds are crucial for the structural rigidity of cellulose fibers. Analysis of the simulation suggests a disrupting effect of Cl^- anions on solvent-exposed intrachain O3H–O5 hydrogen bonds of the fiber, occurring mainly on the hydrophilic surfaces. On origin chains in particular, the probability of hydrogen bond formation is clearly lower than on center chains, as anions interact with the relevant C3-hydroxyls on these chains. These results demonstrate the capability of ILs with a small anion to break cellulose hydrogen bonds and thus to initiate dissolution. In order to assess the effectiveness of Cl^- in disrupting cellulose hydrogen bonds, a comparison of the intrachain hydrogen bond formation of cellulose solvated in BmimCl with that of cellulose solvated in water would be desirable. To this end, we have performed a similar MD simulation of a cellulose fiber solvated in water (TIP3P model (Jorgensen et al. 1983)). This simulation is run for 100 ns at a temperature of 375 K, which corresponds to the boiling temperature of water at which the pretreatment of cellulosic biomass is usually performed. As shown in Fig. S4, the percentage of intramolecular O3H–O5 hydrogen bonds on origin glucan chains is clearly higher in the water simulation (54–68 % on average) than in the BmimCl simulation (25–42 % on average) indicating that the IL is more effective in disrupting solvent-exposed cellulose hydrogen bonds than is water. It should be noted that the lower probability of formed hydrogen bonds in BmimCl may arise from the two simulations being performed at different temperatures, as the formation of hydrogen bonds in cellulose has been shown to be temperature-dependent (Klein et al. 2011; Shen and Gnanakaran 2009). Even so, the present study shows the superiority of ILs over water as a pretreatment solvent for cellulose since they provide a liquid environment at elevated temperatures capable of interfering more severely with cellulose hydrogen bonds, which is not feasible for water at ambient pressure.

The analysis of $Bmim^+$ orientations with respect to different cellulose surfaces revealed two distinct patterns of interaction: stacking on cellulose strands on the hydrophobic surface and intercalation in between cellulose strands on hydrophilic surfaces. The analysis indicates how structural features of the solute and the solvent cation contribute to the favorable interactions with the two. Stacking of $Bmim^+$ on the hydrophobic fiber surface takes place as surface pyranose rings are approached by the planar aromatic imidazole ring. Intercalation of the planar cation in between cellulose chains is facilitated by a differential tilting of center and origin chains on the $(1\bar{1}0)$ surface and by voids on the (010) surface. The stacking interactions with the solvent can facilitate cellulose dissolution by substituting the same kind of interaction between neighboring cellulose layers. It is, however, also conceivable that the intercalation could enhance

the disintegration of cellulose fibers directly through interference with non-polar interactions of neighboring layers and indirectly by promoting the penetration of Cl$^-$ anions into the fiber interior where they can attack intrachain as well as interchain hydrogen bonds essential for fiber integrity. This may provide an explanation how ILs can facilitate cellulose dissolution through interactions on the hydrophilic and hydrophobic fiber surfaces.

The present study reveals how both components of BmimCl interact with the amphiphilic cellulose in the early stages of fiber dissolution. The distinct orientations Bmim$^+$ can adopt on the different surfaces highlight the versatility of imidazolium-based cations, which help to facilitate the disintegration of cellulose layers. Moreover, taking into consideration that Cl$^-$ anions interact extensively with solvent-exposed hydroxyl groups, it is conceivable that cellulose fiber deconstruction is achieved by BmimCl through the combination of polar anions penetrating the fiber and disrupting hydrogen bonds and non-polar cations loosening layers of the cellulose structure via non-polar stacking interactions and intercalation. The present results thus suggest a synergistic approach to cellulose dissolution.

Conclusions

We performed all-atom MD simulations of a cellulose fiber in BmimCl in order to study the role of cations and anions in the initial phase of cellulose dissolution in ILs. The simulations were used to investigate solvent structure around the solute and to identify specific interactions between the two. Selective accumulation of Cl$^-$ anions is found around the solvent-exposed hydroxyl groups of the glucan chains. This contact disrupts intrachain hydrogen bonds on the hydrophilic surface origin chains. In contrast, Bmim$^+$ cations undergo ring stacking interactions with the cellulose hydrophobic surface and intercalate between chains on the hydrophilic surface. Hence, overall, BmimCl solvates cellulose by interacting with both the hydroxyl groups and the hydrophobic side of the polysaccharide, consistent with the Lindman Hypothesis (Medronho et al. 2012; Glasser et al. 2012), and this may explain why ILs act as ideal solvents for the amphiphilic cellulose molecule. Our results are complementary to those from previous simulations on cellulose-IL interactions, in which active roles during dissolution for both anions and cations had been suggested (Cho et al. 2011; Zhao et al. 2012). Moreover, we observe synergistic action of the different ions on different fiber surfaces.

IL treatment of cellulose is known to form non-crystalline aggregates through a dissolution process that involves conformational transformation of the fiber. This process may be governed by distinct interactions between the cellulose and the IL. For example, in a recent experimental study, in which cellulose Iβ was treated with liquid ammonia, large structural changes of the cellulose fiber were found to be induced by specific solute–solvent interactions (Bellesia et al. 2011; Wada et al. 2011). While the results presented here shed light on early events in the dissolution process by ILs, large-scale structural changes of the cellulose fiber, possibly driven by interactions with the IL, remain out of reach due to computational limitation. Therefore, future research on the impact of ILs on cellulose may focus on identifying distinct interaction patterns during experimentally identified different stages of dissolution. Furthermore, in order to realize the full potential of ILs in biomass treatment, further simulations as well as experiments need to be performed to elucidate the effect of ILs on biomass models that include other components, such as lignin and hemicellulose.

References

Alvira P, Tomas-Pejo E, Ballesteros M, Negro MJ (2010) Pretreatment technologies for an efficient bioethanol production process based on enzymatic hydrolysis: a review. Bioresour Technol 101:4851–4861

Bellesia G, Chundawat S, Langan P, Dale B, Gnanakaran S (2011) Probing the early events associated with liquid ammonia pretreatment of native crystalline cellulose. J Phys Chem B 115:9782–9788

BeMiller JN, Whistler L (1996) Carbohydrates. In: Fennema OR (ed) Food chemistry, 3rd edn. CRC, New York, pp 157–224

Berendsen HJC, Postma JPM, van Gunsteren WF, DiNola A, Haak JR (1984) Molecular dynamics with coupling to an external bath. J Chem Phys 81:3684–3690

Bergenstrahle M, Berglund L, Mazeau K (2007) Thermal response in crystalline Ibeta cellulose: a molecular dynamics study. J Phys Chem B 111:9138–9145

Bergenstrahle M, Wohlert J, Himmel M, Brady J (2010) Simulation studies of the insolubility of cellulose. Carbohydr Res 345:2060–2066

Bhargava BL, Balasubramanian S (2007) Refined potential model for atomistic simulations of ionic liquid [bmim] [PF6]. J Chem Phys 127:114510

Bussi G, Donadio D, Parrinello M (2007) Canonical sampling through velocity rescaling. J Chem Phys 126:014101

Chen Y, Stipanovic A, Winter W, Wilson D, Kim Y-J (2007) Effect of digestion by pure cellulases on crystallinity and average chain length for bacterial and microcrystalline celluloses. Cellulose 14:283–293

Cheng G, Varanasi P, Li C, Liu H, Melnichenko Y, Simmons B, Kent M, Singh S (2011) Transition of cellulose crystalline structure and surface morphology of biomass as a function of ionic liquid pretreatment and its relation to enzymatic hydrolysis. Biomacromolecules 12:933–941

Cho H, Gross A, Chu J-W (2011) Dissecting force interactions in cellulose deconstruction reveals the required solvent versatility for overcoming biomass recalcitrance. J Am Chem Soc 133:14033–14041

Chundawat S, Bellesia G, Uppugundla N, da Costa Sousa L, Gao D, Cheh A, Agarwal U, Bianchetti C, Phillips G, Langan P et al (2011) Restructuring the crystalline cellulose hydrogen bond network enhances its depolymerization rate. J Am Chem Soc 133:11163–11174

Dadi A, Varanasi S, Schall C (2006) Enhancement of cellulose saccharification kinetics using an ionic liquid pretreatment step. Biotechnol Bioeng 95:904–910

Dadi A, Schall C, Varanasi S (2007) Mitigation of cellulose recalcitrance to enzymatic hydrolysis by ionic liquid pretreatment. Appl Biochem Biotechnol 137–140:407–421

Darden T, York D, Pedersen L (1993) Particle mesh Ewald: an N*log(N) method for Ewald sums in large systems. J Chem Phys 98:10089–10092

El Seoud O, Koschella A, Fidale L, Dorn S, Heinze T (2007) Applications of ionic liquids in carbohydrate chemistry: a window of opportunities. Biomacromolecules 8:2629–2647

Essmann U, Perera L, Berkowitz M, Darden T, Lee H, Pedersen L (1995) A smooth particle mesh Ewald method. J Chem Phys 103:8577–8593

Fukaya Y, Hayashi K, Kim SS, Ohna H (2010) Design of polar ionic liquids to solubilize cellulose without heating. In: Liebert T, Heinze T, Edgar K (eds) Cellulose solvents: for analysis, shaping and chemical modification, vol 1033. ACS, Washington, pp 55–66

GAUSSIAN version 09 (2009) Wallingford, CT, Gaussian, Inc.

Gericke M, Fardim P, Heinze T (2012) Ionic liquids–promising but challenging solvents for homogeneous derivatization of cellulose. Molecules 17:7458–7502

Glasser WG, Atalla RH, Blackwell J, Brown RM Jr, Burchard W, French AD, Klemm DO, Nishiyama Y (2012) About the structure of cellulose: debating the Lindman Hypothesis. Cellulose 19:589–598

Gray-Weale A (2009) Correlations in the structure and dynamics of ionic liquids. Aust J Chem 62:288–297

Gross A, Chu J-W (2010) On the molecular origins of biomass recalcitrance: the interaction network and solvation structures of cellulose microfibrils. J Phys Chem B 114:13333–13341

Gross A, Bell A, Chu J-W (2012) Entropy of cellulose dissolution in water and in the ionic liquid 1-butyl-3-methylimidazolim chloride. Phys Chem Chem Phys 14:8425–8430

Heinze T, Dorn S, Schöbitz M, Liebert T, Köhler S, Meister F (2008) Interactions of ionic liquids with polysaccharides-2: cellulose. Macromol Symp 262:8–22

Hess B, Bekker H, Berendsen H, Fraaije J (1997) LINCS: a linear constraint solver for molecular simulations. J Comput Chem 18:1463–1472

Hess B, Kutzner C, van der Spoel D, Lindahl E (2008) GROMACS 4: algorithms for highly efficient, load-balanced, and scalable molecular simulation. J Chem Theory Comput 4:435–447

Humphrey W, Dalke A, Schulten K (1996) VMD: visual molecular dynamics. J Mol Graph 14:33–38

Jorgensen W, Chandrasekhar J, Madura J, Impey R, Klein M (1983) Comparison of simple potential functions for simulating liquid water. J Chem Phys 79:926–935

Kim S-J, Dwiatmoko A, Choi J, Suh Y-W, Suh D, Oh M (2010) Cellulose pretreatment with 1-n-butyl-3-methylimidazolium chloride for solid acid-catalyzed hydrolysis. Bioresour Technol 101:8273–8279

Kirschner K, Yongye A, Tschampel S, Gonzalez-Outeirino J, Daniels C, Foley L, Woods R (2008) GLYCAM06: a generalizable biomolecular force field. Carbohydrates. J Comput Chem 29:622–655

Klein H, Cheng X, Smith J, Shen T (2011) Transfer matrix approach to the hydrogen-bonding in cellulose Iα fibrils describes the recalcitrance to thermal deconstruction. J Chem Phys 135:085106

Kowsari MH, Alavi S, Ashrafizaadeh M, Najafi B (2008) Molecular dynamics simulation of imidazolium-based ionic liquids. I. Dynamics and diffusion coefficient. J Chem Phys 129:224508

Langan P, Nishiyama Y, Chanzy H (1999) A revised structure and hydrogen-bonding system in cellulose II from a neutron fiber diffraction analysis. J Am Chem Soc 121:9940–9946

Langan P, Nishiyama Y, Chanzy H (2001) X-ray structure of mercerized cellulose II at 1 Å resolution. Biomacromolecules 2:410–416

Langan P, Gnanakaran S, Rector K, Pawley N, Fox D, Cho D, Hammel K (2011) Exploring new strategies for cellulosic biofuels production. Energy Environ Sci 4:3820–3833

Li C, Knierim B, Manisseri C, Arora R, Scheller H, Auer M, Vogel K, Simmons B, Singh S (2010) Comparison of dilute acid and ionic liquid pretreatment of switchgrass: biomass recalcitrance, delignification and enzymatic saccharification. Bioresour Technol 101:4900–4906

Lindman B, Karlström G, Stigsson L (2010) On the mechanism of dissolution of cellulose. J Mol Liq 156:76–81

Liu L, Chen H (2006) Enzymatic hydrolysis of cellulose materials treated with ionic liquid [BMIM] Cl. Chin Sci Bull 51:2432–2436

Liu Z, Huang S, Wang W (2004) A refined force field for molecular simulation of imidazolium-based ionic liquids. J Phys Chem B 108:12978–12989

Liu C, Sun R, Zhang A, Li W (2010a) Dissolution of cellulose in ionic liquids and its application for cellulose processing and modification. In: Liebert T, Heinze T, Edgar K (eds)

Cellulose solvents: for analysis, shaping and chemical modification, vol 1033. ACS, New York, pp 287–297

Liu H, Sale K, Holmes B, Simmons B, Singh S (2010b) Understanding the interactions of cellulose with ionic liquids: a molecular dynamics study. J Phys Chem B 114:4293–4301

Liu H, Sale K, Simmons B, Singh S (2011) Molecular dynamics study of polysaccharides in binary solvent mixtures of an ionic liquid and water. J Phys Chem B 115:10251–10258

Lucas M, Wagner G, Nishiyama Y, Hanson L, Samayam I, Schall C, Langan P, Rector K (2011) Reversible swelling of the cell wall of poplar biomass by ionic liquid at room temperature. Bioresour Technol 102:4518–4523

Margulis CJ, Stern HA, Berne BJ (2002) Computer simulation of a "Green Chemistry" Room-temperature ionic solvent. J Phys Chem B 106:12017–12021

MATLAB version 7.12.0 (2011) Natick, Massachusetts: The MathWorks Inc.

Matthews J, Skopec C, Mason P, Zuccato P, Torget R, Sugiyama J, Himmel M, Brady J (2006) Computer simulation studies of microcrystalline cellulose Iß. Carbohydr Res 341:138–152

Matthews J, Himmel M, Brady J (2010) Simulations of the structure of cellulose. In: Nimlos MR, Crowley MF (eds) Computational modeling in lignocellulosic biofuel production, vol 1052. ACS Symposium Series, pp 17–53

Matthews J, Bergenstrahle M, Beckham G, Himmel M, Nimlos M, Brady J, Crowley M (2011) High-temperature behavior of cellulose I. J Phys Chem B 115:2155–2166

Medronho B, Romano A, Miguel M, Stigsson L, Lindman B (2012) Rationalizing cellulose (in)solubility: reviewing basic physicochemical aspects and role of hydrophobic interactions. Cellulose 19:581–587

Mostofian B, Smith JC, Cheng X (2011) The solvation structures of cellulose microfibrils in ionic liquids. Interdiscip Sci Comput Life Sci 3:308–320

Moulthrop J, Swatloski R, Moyna G, Rogers R (2005) High-resolution ^{13}C NMR studies of cellulose and cellulose oligomers in ionic liquid solutions. Chem Commun 12:1557–1559

Muldoon M, Gordon C, Dunkin I (2001) Investigations of solvent-solute interactions in room temperature ionic liquids using solvatochromic dyes. J Chem Soc Perkin Trans 2:433–435

Nishiyama Y, Langan P, Chanzy H (2002) Crystal structure and hydrogen-bonding system in cellulose Iß from synchrotron X-ray and neutron fiber diffraction. J Am Chem Soc 124:9074–9082

Nishiyama Y, Sugiyama J, Chanzy H, Langan P (2003) Crystal structure and hydrogen bonding system in cellulose Iα from synchrotron X-ray and neutron fiber diffraction. J Am Chem Soc 125:14300–14306

Ohira K, Abe Y, Kawatsura M, Suzuki K, Mizuno M, Amano Y, Itoh T (2012) Design of cellulose dissolving ionic liquids inspired by nature. ChemSusChem 5:388–391

Raju SG, Balasubramanian S (2010) Role of cation symmetry in intermolecular structure and dynamics of room temperature ionic liquids: simulation studies. J Phys Chem B 114:6455–6463

Ramadugu S, Chung Y-H, Xia J, Margulis C (2009) When sugars get wet. A comprehensive study of the behavior of

water on the surface of oligosaccharides. J Phys Chem B 113:11003–11015

Reichardt C (2005) Polarity of ionic liquids determined empirically by means of solvatochromic pyridinium N-phenolate betaine dyes. Green Chem 7:339–351

Rinaldi R, Palkovits R, Schüth F (2008) Depolymerization of cellulose using solid catalysts in ionic liquids. Angew Chem Int Ed 47:8047–8050

Samayam I, Hanson L, Langan P, Schall C (2011) Ionic-liquid induced changes in cellulose structure associated with enhanced biomass hydrolysis. Biomacromolecules 12:3091–3098

Sellin M, Ondruschka B, Stark A (2010) Hydrogen bond acceptor properties of ionic liquids and their effect on cellulose solubility. In: Liebert T, Heinze T, Edgar K (eds) Cellulose solvents: for analysis, shaping and chemical modification, vol 1033. ACS, New York, pp 121–135

Shen T, Gnanakaran S (2009) The stability of cellulose: a statistical perspective from a coarse-grained model of hydrogen-bond networks. Biophys J 96:3032–3040

Sun N, Rodriguez H, Rahman M, Rogers R (2011) Where are ionic liquid strategies most suited in the pursuit of chemicals and energy from lignocellulosic biomass? Chem Commun 47:1405–1421

Swatloski R, Spear S, Holbrey J, Rogers R (2002) Dissolution of cellose with ionic liquids. J Am Chem Soc 124:4974–4975

Urahata S, Ribeiro M (2005) Single particle dynamics in ionic liquids of 1-alkyl-3-methylimidazolium cations. J Chem Phys 122:024511

Wada M, Nishiyama Y, Bellesia G, Forsyth T, Gnanakaran S, Langan P (2011) Neutron crystallographic and molecular dynamics studies of the structure of ammonia-cellulose I: rearrangement of hydrogen bonding during the treatment of cellulose with ammonia. Cellulose 18:191–206

Wang H, Gurau G, Rogers R (2012) Ionic liquid processing of cellulose. Chem Soc Rev 41:1519–1537

Youngs TGA, Hardacre C, Holbrey JD (2007) Glucose solvation by the ionic liquid 1,3-dimethylimidazolium chloride: a simulation study. J Phys Chem B 111:13765–13774

Yui T, Nishimura S, Akiba S, Hayashi S (2006) Swelling behavior of the cellulose Iβ crystal models by molecular dynamics. Carbohydr Res 341:2521–2530

Zavrel M, Bross D, Funke M, Buechs J, Spiess A (2009) High-throughput screening for ionic liquids dissolving (ligno-)cellulose. Bioresour Technol 100:2580–2587

Zhang Y, Chan J (2010) Sustainable chemistry: imidazolium salts in biomass conversion and CO_2 fixation. Energy Environ Sci 3:408–417

Zhang L, Ruan D, Gao S (2002) Dissolution and regeneration of cellulose in NaOH/thiourea aqueous solution. J Polym Sci B Polym Phys 40:1521–1529

Zhao Y, Liu X, Wang J, Zhang S (2012) Effects of cationic structure on cellulose dissolution in ionic liquids: a molecular dynamics study. ChemPhysChem 13:3126–3133

Zhu S, Wu Y, Chen Q, Yu Z, Wang C, Jin S, Ding Y, Wu G (2006) Dissolution of cellulose with ionic liquids and its application: a mini-review. Green Chem 8:325–327